HIL Test of Power System Frequency Control by Electric Vehicles

Hidekuni Toda, Yutaka Ota, Tatsuhito Nakajima
Department of Electrical and Electronic Engineering
Tokyo City University
Tokyo, Japan
g1781343@tcu.ac.jp

Ken-ichi Kawabe
Department of Electrical and Electronic Engineering
Tokyo Institute of Technology
Tokyo, Japan

Akihiko Yokoyama
Department of Advanced Energy
The University of Tokyo
Tokyo, Japan

***Abstract*—As the introduction amount of renewable energy increases, frequency fluctuation is regarded as a problem. On the other hand, since the pure plug-in electric vehicle (PEV) and the plug-in hybrid electric vehicles (PHEV) are becoming widespread, V2G is getting real. In this paper, two control schemes, centralized LFC and autonomous FFR, were implemented to the vehicle grid integration HIL. Control performance including measurements, communication delays, and other actual implementation conditions was evaluated through the closed loop HIL tests with the EV battery and PCS system. It was founded that carefully coordinated system in the laboratory was enough to accommodate the FFR that is one of the advanced ancillary services by the demand side equipment.**

Keywords-component; Power System; Electric Vehicle(EV); Vehicle to Grid(V2G); Frequency Control; Hardware In the Loop(HIL); Smart Grid

I. INTRODUCTION

In recent years, vehicles equipped with batteries such as the pure plug-in PEV and PHEV are becoming widespread. Driving distance in normal days is relatively short, so it can be said that V2G is getting real. Various V2G control schemes have been proposed by the simulation study [1], [2], and demonstration projects receiving ancillary service signal from the utility [3], [4]. The authors think it is important to consider the interactions among the battery and inverter control responses, communication delays in case of remote control, and power system frequency dynamics including impacts of the V2G control.

In this paper, we tests two V2G control schemes through the HIL(Hardware In the Loop) consisted by a real-time power system simulator assuming massive integration of renewable energy generations and PEVs into the power system, an actual PEV battery energy storage, and V2G capable power conditioning system (PCS). Effectiveness of the PEV-FFR (Fast Frequency Response) featuring quick response of the PEV battery and inverter system, PEV-LFC (Load Frequency Control) coordinating large-scale thermal generations are evaluated by HIL test, respectively.

II. HIL CONFIGURATION AND MODELS

A. Overview of the HIL

Fig. 1 shows component of the HIL, and Fig. 2 shows the experimental setup in our laboratory. The power HIL targeting the EV battery and PCS system [5] is conducted by the frequency fluctuation calculation on the real-time simulator and the power amplifier. In case of PEV-LFC, communication HIL is conducted through the laboratory Ethernet.

The frequency command value calculated by the frequency analysis model implemented in the real-time simulator (OPAL-RT Technology, OP 5600) is transmitted to the power amplifier (California Instruments, MX 15, rated: 15 kVA), and the power amplifier reflects the frequency variation value and outputs the instantaneous voltage value. For PEV-FFR, the EV controller (dSPACE, Micro Auto Box II) measures the frequency and issues a V2G command to the EV battery (Mitsubishi Motors Corporation, i-MiEV, capacity: 16 kWh) and the PCS (NICHICON, NECST-TD1) system. For PEV-LFC, the EV controller receives the LFC power commands from the real-time simulator via Ethernet. In both case, the PCS control charging or discharging power to the power amplifier. By feeding back measured value of the active power to the real-time simulator, the frequency fluctuation calculation of the next step is performed. This series of operations is repeated in real time.

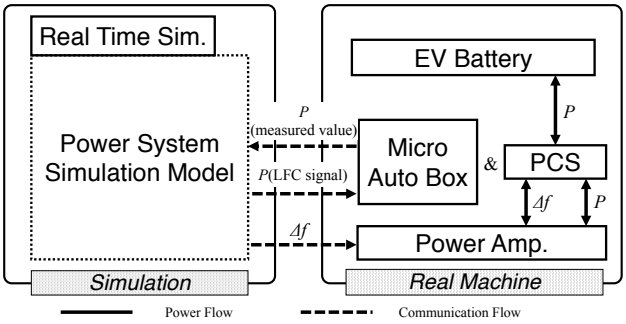

Figure 1. Component of the HIL

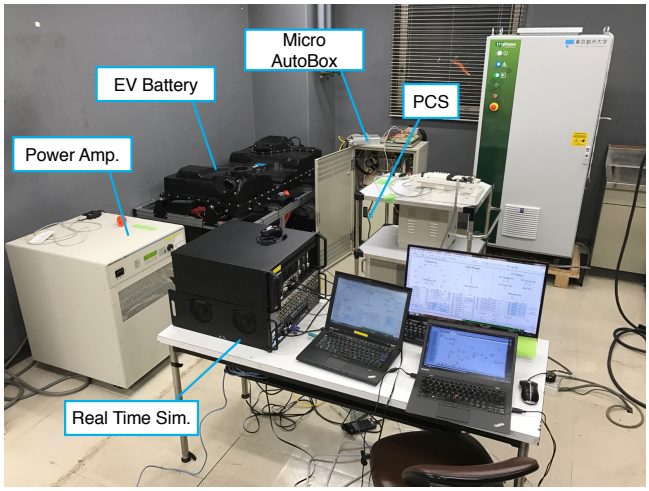

Figure 2. Experimental setup of the HIL.

B. *Case assumption*

The following two control cases are assumed as HIL test : (Case1) EV is controlled by the emulated LFC signal in the real-time simulator, that corresponds PEV-LFC (Case2) EV is controlled based on local frequency measurements, that corresponds PEV-FFR.

For each control case, (a) HIL simulation with the EV and PCS system, (b) Real-time simulation with ideal EV response inside the model, (c) Real-time simulation without EV control are performed at the same time. Contribution of communication delay and control response on the control performance can be evaluated.

C. *Power system model*

The power system model is assumed to be a prefecture level with a population of about 9 million people. Supply and demand imbalance (ΔP) is calculated by a thermal power generator with EDC (Economic Dispatch Control) and LFC, the PV modeled as natural variation on active power, the aggregated load based on historical measurements, and the EV system, as shown in Fig. 3. The frequency deviation ($\Delta \omega$) is estimated considering the power system inertia constant (M) and the power system damping constant (D). In this paper, system inertia and damping is set as 9[s], 2[p.u.], respectively.

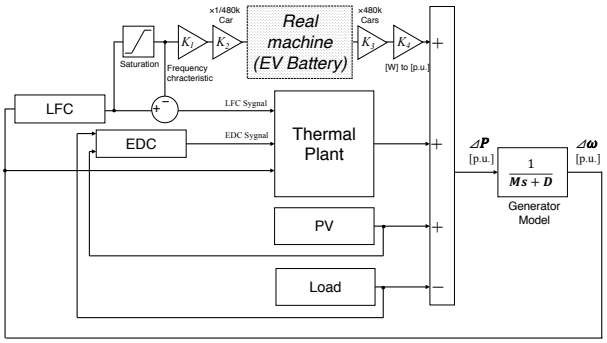

(a) For Case1 (LFC)

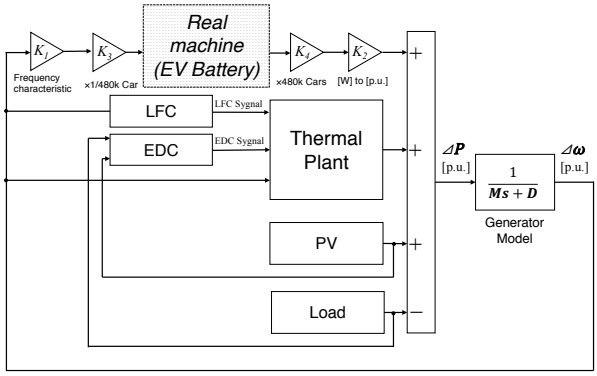

(b) For Case2 (FFR)

Figure 3. Power system model

Fig. 4. shows the thermal power generator model consists of a turbine and a speed governor, and the parameters are summarized in Table. I [5]. The power output of the thermal power generator is determined based on the EDC, the LFC, and the governor free control. Rate limiter of the LFC and the EDC is 5 [% p.u./min], respectively. The power capacity for the governor-free control and the LFC is 5 [%] and 1.5 [%] on the system capacity, respectively.

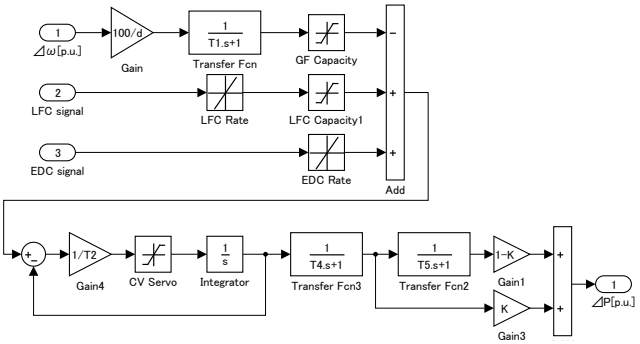

Figure 4. Thermal power generator model

TABLE I. PARAMETERS OF THERMAL POWER GENERATOR

d	***Permanent Speed Variation [%]***	5
T_1	***Speed Relay Time Constant [s]***	0.2
T_2	***CV Servo Time Constant [s]***	0.2
T_3	***CV Servo Open Time [s]***	5
T_4	***High Pressure Turbine Time Constant [s]***	0.25

T_5	***Low Pressure Turbine Time Constant [s]***	9.0
T_6	***CV Servo Close Time [s]***	-0.001
K	***High Pressure Output Dispatching Rate [p.u.]***	0.3

The EDC signal is calculated from the difference between the demand fluctuation and PV output. Zero-order hold time is 5 [s], and the time constant of the first order lag is set to 30 seconds.

Fig. 5. shows the LFC system model, and the parameter for the LFC is summarized in Table. II. The PI control with anti-windup function is considered to the area requirement estimated by the frequency deviation. In Case2 (LFC), the generated LFC signal is preferentially dispatched to the EV, and residual signal is also dispatched to the thermal power generator.

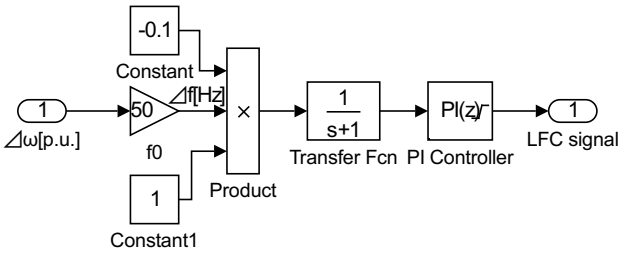

Figure 5. LFC system model

TABLE II. PARAMETERS FOR LFC

T_{AR}	***Calculation Cycle Time of Area Requirement [s]***	1
K_p	***PI Controller Proportional Gain [p.u.]***	1
T_i	***PI Controller Integral Gain [p.u.]***	0.1

D. EV model

The number of passenger cars owned in the target region is about 3 million. The 2030 target ratio of EV to the total stocks is about 16[%]. Therefore, we assumed the number of EVs to be about 480 thousand. The battery capacity of EV is 16 [kWh] and the V2G power is 3 [kW] on the EV test system.

In Case 1 (LFC), V2G power is determined by the LFC signal. It is assumed that all the EVs receive the same LFC signal. In Case 2, V2G power is determined by the frequency deviation. Autonomous droop control with 2000 [W/Hz] gain is implemented to the modeled EV and the actual EV battery and PCS system.

E. Dataset of PV and Load

Fig.6 shows dataset of PV power generation and load consumption during a cloudy day. The measurements of actual PV site in every second are used for the HIL. The introduction rate is assumed as 20% of the system capacity considering Japanese 2030 target. Due to the smoothing effect is not taken into consideration and the introduction rate is large, the simulated frequency deviation is much higher than that of the current power systems.

The daily trend of the load consumption is generated by using historical dataset published by TEPCO (Tokyo Electric Power Company) [6], [7]. Amount of the load is proportionally divided to a prefecture level. Short cycle load fluctuation is interposed as white noise. Their standard deviation is determined as following well-known relationship.

$$\sigma_D = \gamma\sqrt{P_{demmand}} \quad (1)$$

Where, γ is set to 0.9 in this paper.

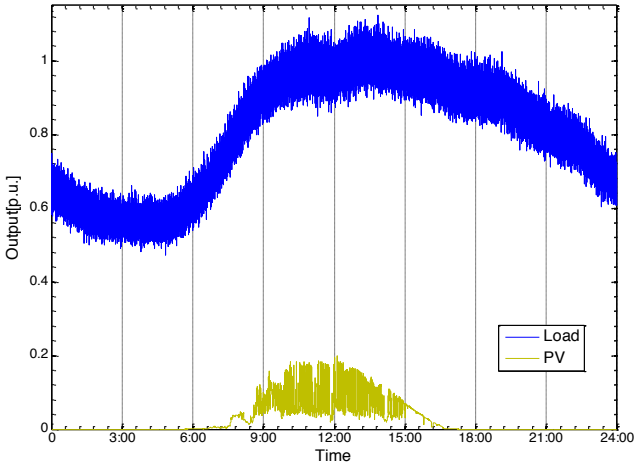

Figure 6. Dataset of PV and Load

The PV and load dataset of 300 seconds from 13:05 to 13:10 is used for the HIL test because the fluctuation components are significant. Dataset in every second is down sampled, and inputted to the 50Hz power system model. Sampling time of the HIL simulation is 0.01[s], it is enough for considering generator dynamics.

III. RESULTS

The frequency fluctuations of Case 1, Case 2 are summarized in Fig. 7, Fig. 8, respectively. Frequency fluctuations are obvious suppressed by the EV control. In Case 1, experimental results of the HIL is slightly deteriorated as simulated ideal results. This is mainly caused by communication delays for sending LFC signals to the EV PCS. In Case2, difference between the experiment and the ideal simulation is not so significant. This result shows that system latency consists of the local frequency measurement and EV PCS response is enough to accommodate the FFR.

Comparing the cases of experimental result by the HIL as shown in Fig. 9, Case 2 have better performance than Case 1 because there is no communication delays in Case 2. However, it can be said control performance is changeable under various frequency droop gain setting.

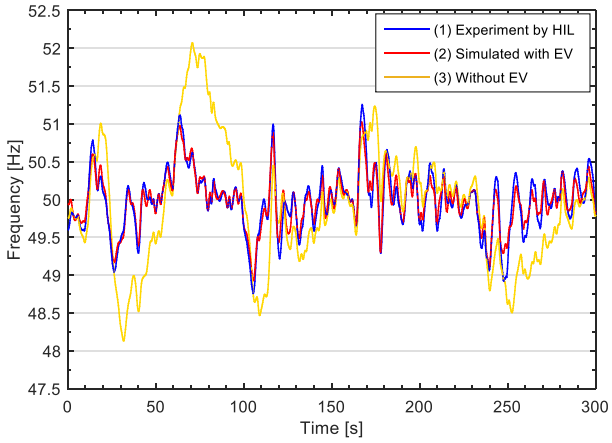

Figure 7. Frequency fluctuation (Case1)

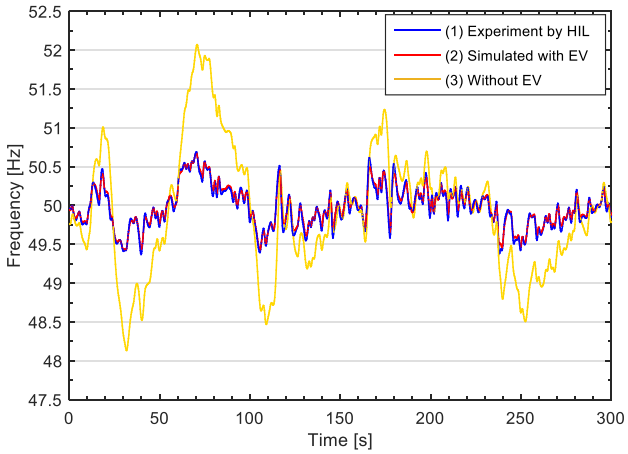

Figure 8. Frequency fluctuation (Case2)

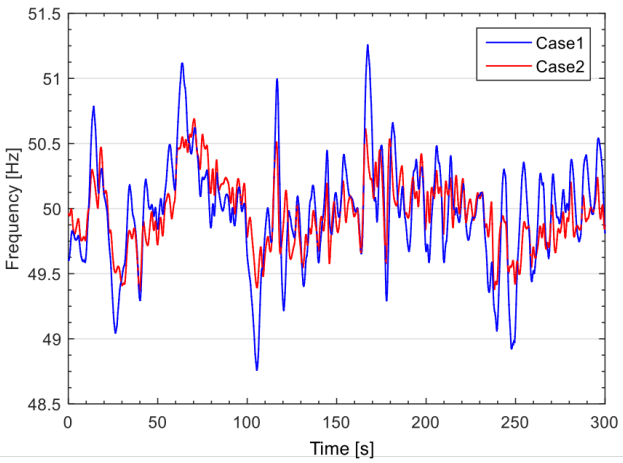

Figure 9. Frequency fluctuation (Case1 vs Case2)

The original potential of control performance and deterioration of control performance in actual implementation can be quantified by executing the HIL simulation and ideal online simulation at the same time. Control performances are evaluated from the RMS of the frequency fluctuation and maximum values of the frequency deviation, as shown in Fig. 10, Fig. 11, Fig. 12, and Fig. 13. The FFR shows better performance both in the RMS and maximum values under the HIL conditions and dataset in this paper.

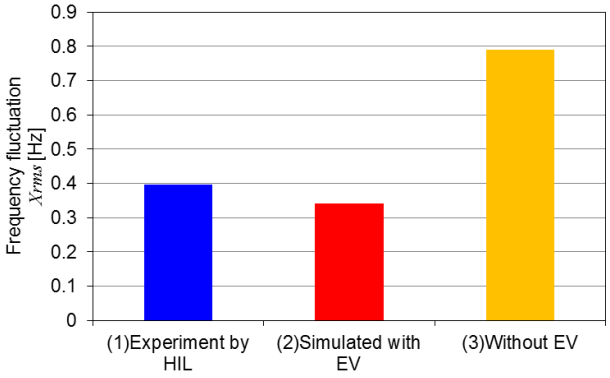

Figure 10. RMS of frequency fluctiation (Case1)

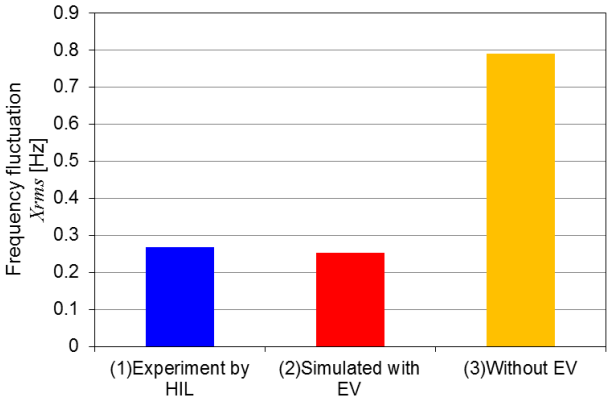

Figure 11. RMS of frequency fluctuation (Case2)

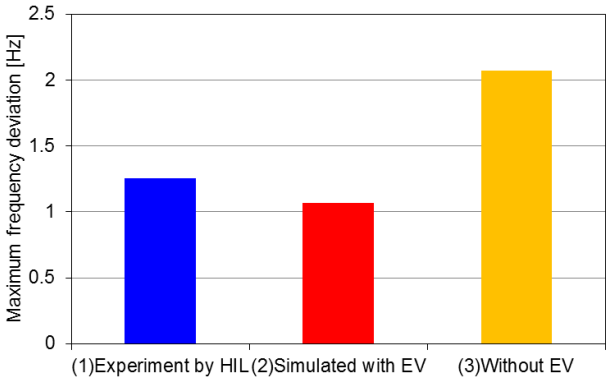

Figure 12. Maximum of frequency deviation (Case1)

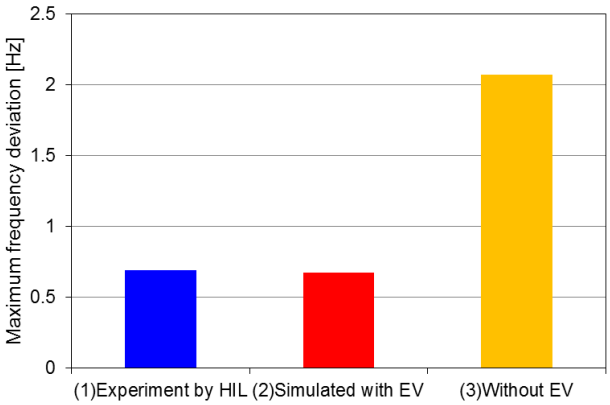

Figure 13. Maximum of frequency deviation (Case2)

Fig 12. and Fig 13. are comparisons of the maximum deviation of frequencies. The maximum frequency deviation was similar to that of RMS.

When looking at the whole, it can be said that Case 2 operates closer to simulation.

IV. CONCLUSION

In this paper, two control schemes, centralized LFC and autonomous FFR, were implemented to the vehicle grid integration HIL. Control performance including measurements, communication delays, and other actual implementation conditions was evaluated through the closed loop HIL tests with the EV battery and PCS system. It was founded that carefully coordinated system in the laboratory was enough to accommodate the FFR that is one of the advanced ancillary services by the demand side equipment.

Real-time emulation function of the ancillary service signals under massive renewable integration would be effective for various pilot projects of the virtual power plant. The authors are preparing some demonstration projects.

In this time, the FFR was performed on the HIL environment. We prepare to evaluate performance of the synthetic inertia response (SIR) based on *df/dt* measurements. Optimal dispatching the LFC, FFR, and SIR to multiple EVs with different system response and battery state-of-charge is our next research target.

ACKNOWLEDGMENT

This work was supported by JSPS KAKENHI 15H03958, 17K06316 and JST CREST JPMJCR15K3.

REFERENCES

[1] M. D. Galus, S. Koch, and G. Andersson, “Provision of Load Frequency Control by PHEVs, Controllable Loads, and a Cogeneration Unit”, IEEE Trans. Industrial Electronics, Vol.58, Issue.10, pp.4568-4582 (2011)

[2] E. Sortomme and M. A. El-Sharkawi, “Optimal Combined Bidding of Vehicle-to-Grid Ancillary Services”, IEEE Trans. Smart Grid, Vol.3, Issue.1, pp.70-79 (2012)

[3] University of Delaware, “The Grid-Integrated Vehicle with Vehicle to Grid Technology”, http://www1.udel.edu/V2G/

[4] The Parker Project, http://parker-project.com

[5] Y. Ota, H. Taniguchi, J. Baba, and A. Yokoyama, "Implementation of Autonomous Distributed V2G to Electric Vehicle and DC Charging System", Electric Power Systems Research, Vol.120, pp.177–183 (2015)

[6] IEEJ Japanese Power System Models, http://www.iee.jp/pes/?page_id=141

“Load Frequency Control of Power System in Normal and Emergency Case”, IEEJ Technical Report, No.869, 2002. (in Japanese)

[7] “Past power usage record data download | Electric weather forecast”, TEPCO Power Grid, Incorporated, http://www.tepco.co.jp/forecast/html/download-j.html [January 2017]. (in Japanese)

[8] “ Business scale by region | Viewed in a table by TEPCO”, Tokyo Electric Power Company Holdings, Incorporated, http://www.tepco.co.jp/corporateinfo/illustrated/business/business-scale-area-j.htm [January 2017]. (in Japanese)